

A Variational Pseudo-Observation Guided Nudged Particle Filter

Theofania Karampela and Ryne Beeson 
 Mechanical and Aerospace Engineering
 Princeton University
 Princeton, New Jersey, USA
 tk4161@princeton.edu and ryne@princeton.edu

Abstract—Nonlinear filtering with standard Particle Filter (PF) methods requires mitigative techniques to quell weight degeneracy, such as resampling. This is especially true in high-dimensional systems with sparse observations. Unfortunately, such techniques are also fragile when applied to systems with exceedingly rare events. Nonlinear systems with these properties can be assimilated effectively with a control-based PF method known as the Nudged Particle Filter (nPF), but this method has a high computational cost burden. In this work, we aim to retain this strength of the nudged method while reducing the computational cost by introducing a variational method into the algorithm that acts as a continuous pseudo-observation path. By maintaining a PF representation, the resulting algorithm continues to capture an approximation of the filtering distribution, while reducing computational runtime and improving robustness to the “rare” event of switching phases. Preliminary testing of the new approach is demonstrated on a stochastic variant of the nonlinear and chaotic Lorenz 1963 (L63) model, which is used as a surrogate for mimicking “rare” events. The new approach helps to overcome difficulties in applying the nPF for realistic problems and performs favorably with respect to a standard PF with a higher number of particles.

Index Terms—Particle Filter, Nudged Particle Filter, Variational Method, Variational Nudged Particle Filter, Optimal Importance Sampling, Lorenz 1963, Rare Events

I. INTRODUCTION

In this manuscript we are interested in the filtering solution to partially observable continuous-time signal processes (X_t) with discrete-time observations (Y_{t_k})

$$\begin{aligned} dX_t &= f(X_t)dt + \sigma(X_t)dW_t, & X_0 &= x \in \mathbb{R}^m, \\ Y_{t_k} &= h(X_{t_k}) + \xi_{t_k}, & Y_0 &= 0 \in \mathbb{R}^d, \end{aligned} \quad (1)$$

where (t_k) is an increasing sequence of observation times indexed by $k \in \mathbb{N}$ with $t_0 = 0$, and $\xi_{t_k} \sim \mathcal{N}(0, \Sigma_y)$ is the observation noise that is independent of the standard Brownian motion (BM) W_t that drives the signal process X_t . We denote the filtering solution of X at time t given the observations up to time $t_k \leq t$ by $p_t(x|\mathcal{F}_k^Y)$. We use \mathcal{F}_k^Y to denote all observations up to time t_k (simplifying the subscript from t_k to just k for brevity here and in what follows) and hence the prior conditional distribution at time t_k is $p_k(x|\mathcal{F}_{k-1}^Y)$ and the posterior is $p_k(x|\mathcal{F}_k^Y)$.

Additional properties that we assume of (1), and that drive choices in filtering algorithms and the method developed in this work, is that X represents a state of very high dimension

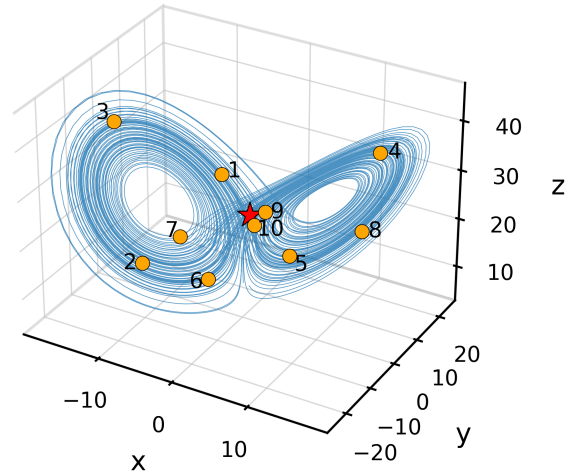


Fig. 1: L63 deterministic attractor with initial conditions (see Table III) used in numerical experiments (see §IV).

(e.g., in the extreme cases of geophysical data assimilation [1], [2], this can be $m \sim O(10^8)$ degrees of freedom that results from the discretization of partial differential equations (PDEs) describing physical processes), that the prior and posterior distributions are non-Gaussian, that the numerical solution of the signal process given in (1) is computationally demanding, and lastly, that intermittent aperiodic behavior characteristic of rare events takes place. A rare event is one that is represented by a low probability of occurrence; often associated with a state X in the tail of the distribution $p(x|\mathcal{F}^Y)$. Geophysical models generally possess the first three properties [1], [3], and examples of rare events include hurricanes, earthquakes, and rapid overturning in ocean flows [4], [5], [6]. Filtering problems with these characteristics lead naturally to methods of either a variational or a low-sample ensemble-based approach.

Variational methods provide a smoothing solution for the maximum a posteriori (MAP) state [3], [7], [8]. Their disadvantage is that they only provide a MAP state and not a representation of the full distribution or even higher-order moments. Lastly, because of the computational difficulty of solving such problems for high-dimensional systems, parameters that should be state and time varying are often fixed to

static background (or climatological) values and hence do not represent the true near term variability.

An alternative solution is to approximate the filtering distribution with an importance sampling approach. With $((X^i, w^i) \sim p)_{i=1}^N$ representing $N \in \mathbb{N}$ pairs of samples (X^i) with normalized weights (w^i) from a distribution p , the N -ensemble approximation p^N to p is

$$p^N(dx) \equiv \sum_{i=1}^N w^i \delta_{X^i}(dx) \approx p(dx), \quad (2)$$

where δ_{X^i} is the Dirac distribution at X^i . The class of PF methods allow the weights to change during assimilation cycles; a reflection of the fact that they are importance weights. In the standard approach, the particle locations remain fixed during the Bayesian update. As we will recall in §II, the adjustment of the particle weights at times of filtering updates is what ultimately leads to the well known issue of particle degeneracy. Some recent efforts in the literature navigate the issue of particle degeneracy by maintaining equal weights during Bayes' update by reframing the discrete-time update as a flowing of the particles in the state-space during a pseudo-observation interval [9], [10], [11], solving for an equivalent flow map [12], [13], or an implicit mapping [14]. Additionally, comments on how the flow-based approaches distinguish themselves from the main method of this paper, based on the nPF, will be given in §II.

There are filtering methods that are ensemble-based, where the weights are chosen as equal (i.e., $w^i = 1/N$) and remain equal throughout the filtering update. Common families of these methods include the well-known variants of the Ensemble Kalman Filter (EnKF) [15], [16], Unscented Kalman Filter (UKF) [17], and Gaussian Mixture Model (GMM) [18]. Although these methods provide a built-in protection from particle degeneracy, just as the flow-based and flow-map PF methods do, these approaches do not provide the flexibility to account for modified particle dynamics between observations which would be reflected in varying importance weights; this is an essential characteristic of the nPF and provides greater ability to adapt to problems with nonlinear dynamics or "rare" events.

When $N \ll m$, the distribution p^N is unlikely to have state representations in the tails of p , and therefore methods that generate the prior distribution by advecting each particle under the dynamics given by (1) are likely to result in a prior that does not have support containing the true state in the case of a "rare" event. If instead the particles are allowed to adjust their paths to reflect the most likely path between observations; for instance, by introducing a control u_t to the dynamics

$$dX_t = f(X_t)dt + u_t dt + \sigma(X_t)dW_t, \quad (3)$$

then the posterior distribution at one time can be effectively steered to a representative prior distribution even in the presence of these "rare" events.

The approach of (3) is the approach for the nPF [19], [20] that this work builds upon and will be recalled in §II. The

nPF was originally proposed for mitigating weight degeneracy of the standard PF in nonlinear chaotic and sparse filtering problems, but also has the required formulation to address the "rare" event problem. The central drawback of the nPF is that the exact control solution, which is continuous in time, is often approximated by Monte Carlo (MC) approaches that converge slowly, and hence it is computationally burdensome. The aim of this manuscript is to test the efficacy of using a hybrid Variational nudged Particle Filter (Var-nPF) approach, whereby the variational method is used to generate a pseudo-observation path that provides state-space guidance of the nPF particles.

As will become clear in the explanations contained in §III, this allows for a shorter time horizon optimal control problem to be solved for the nPF and hence provides an avenue to reduce its computational cost, while still maintaining the ability to approximate the filtering distribution at all times and handle the case of "rare" events.

The paper now proceeds as follows. In §II we recall the basics of the standard bootstrap PF and provide background on the nPF. We provide relevant citations to the literature in this section for those methods and set notation. In §III we detail the variational approach used in this work and the new method that combines it with the nPF. In §IV we provide the model setup for a stochastic L63 system, shown in Fig. 1, that will serve as a surrogate to mimic "rare" events in geophysical problems. Simulation results are also given and discussed in this section. Final remarks and future efforts are given in §V.

II. STANDARD AND NUDGED PARTICLE FILTER

A. Standard Particle Filter

The standard (bootstrap) PF [21], with resampling proceeds in three distinct steps (prior, Bayes' update, and resampling) that repeat for each observation cycle. We assume that we start with an N -particle approximation of the posterior distribution at time t_{k-1} with normalized weights $\sum_{i=1}^N w^i = 1$, as expressed in (2). The standard PF with resampling then proceeds recursively by generating the prior at time t_k by advecting each particle X_{k-1}^i under the dynamics given in (1) to time t_k

$$p_k^N(dx|\mathcal{F}_{k-1}^Y) = \sum_{i=1}^N w_{k-1}^i \delta_{X_k^i}(dx). \quad (4)$$

Then, given the observation Y_k , unnormalized weights are calculated according to Bayes' formula

$$\tilde{w}_k^i = w_{k-1}^i p_k(Y_k|X_k^i), \quad (5)$$

where $p_k(Y_k|X_k^i)$ is the likelihood function associated with the measurement process given in (1). After normalizing these weights $w_k^i = \tilde{w}_k^i / \sum_{i=1}^N \tilde{w}_k^i$, the posterior distribution at time t_k is as

$$p_k^N(dx|\mathcal{F}_k^Y) \equiv \sum_{i=1}^N w_k^i \delta_{X_k^i}(dx). \quad (6)$$

Lastly, if the particle weights are degenerate (i.e., the variance of the weights is large), then the particles are independently

and identically resampled from the particle set (X_k^i) with probability according to the normalized weights (w_k^i) . This process results in particles that may have the same support locations, but now with equal weights (i.e., $w_k^i = 1/N$).

To determine whether the particle approximation is degenerate in this work, we use an approximation of the Effective Sample Size (ESS) [22], [23]. With the vector of normalized weights denoted as w , the approximation is given by

$$N_{\text{eff}} \equiv 1/\langle w, w \rangle.$$

We use the threshold of $N_{\text{eff}} < N/2$ to trigger resampling with the universal (or systematic) resampling approach [24].

B. Nudged Particle Filter

The key difference between the nPF and a standard PF algorithm is that the particles are advected under the dynamics given by (3) as opposed to (1). The forcing u_t is a nonlinear control law that is obtained independently for each particle X^i by solving a finite-time horizon optimal control problem (OCP) that is dependent on the new observation. The result of applying the control is that particles are *nudged* toward the area of high likelihood for the new observation. The setup and main result of this OCP are given in the following theorem statement.

Notation: The superscript notation $X^{k,x}$ for any particle indicates an initial condition at $x \in \mathbb{R}^m$ at time t_k . $C([t_k, t_{k+1}])$ is the space of continuous functions and a superscript asterisk (e.g., σ^*) indicates the transpose of a matrix.

Theorem II.1 (Nudged Particle Filter (nPF)) [19], [20]

Given a sample $X_{t_k}^{k,x} \sim p_k^N(dx|\mathcal{F}_k^Y)$ and observation Y_{k+1} , the solution of the OCP

$$\begin{aligned} & \min_{u \in C([t_k, t_{k+1}])} \{J(u; k, x, Y_{k+1}) \\ & \equiv \mathbb{E} \left[\int_{t_k}^{t_{k+1}} \frac{1}{2} \langle u_s, R_s^{-1} u_s \rangle ds + g(X_{k+1}^{k,x}, Y_{k+1}) \right] \}, \quad (7) \end{aligned}$$

with dynamic constraint for $X_t^{k,x}$, $t \in [t_k, t_{k+1})$ given by (3), g the log-likelihood of the observation, R_s the diffusion matrix of the stochastic forcing in (3), is (under reasonable assumptions) a feedback control law

$$u(t, x) = \frac{1}{\Phi(t, x)} R_t \nabla_x \Phi(t, x), \quad (8)$$

with Φ and $\nabla_x \Phi$ solutions to linear parabolic PDEs that can be written in terms of Feynman-Kac relations

$$\Phi(t, x) = \mathbb{E} \left[\exp(-g(\eta_{k+1}^{k,x}, Y_{k+1})) \right], \quad (9)$$

and

$$\begin{aligned} \nabla_x \Phi(t, x) &= -\mathbb{E} \left[\exp(-g(\eta_{k+1}^{k,x}, Y_{k+1})) \right. \\ & \left. \exp \left(\int_{t_k}^{t_{k+1}} \nabla_x f(\eta_s^{k,x}) ds \right) \nabla_x g(\eta_{k+1}^{k,x}, Y_{k+1}) \right], \quad (10) \end{aligned}$$

with $\eta_{k+1}^{k,x}$ being realizations of (1).

An important result of the control solution given in (8) is that particles attempt to stay faithful to the modeled dynamics of (1). Any deviation is accounted for by a change in their unnormalized weights.

Corollary II.1 (nPF Radon-Nikodym Derivative) [20]

The unnormalized weights of the sample $X_t^{k,x}$ under the control law (8) given by Theorem II.1 change according to the continuous-time Radon-Nikodym derivative

$$\begin{aligned} \frac{d\mu^i}{d\widehat{\mu}^i} \Big|_{t \in [t_k, t_{k+1}]} &= \exp \left(- \int_{t_k}^t \langle v(s, X_s^i), dW_s \rangle \right. \\ & \left. - \frac{1}{2} \int_{t_k}^t \langle v(s, X_s^i), v(s, X_s^i) \rangle ds \right), \quad (11) \end{aligned}$$

where $v(s, X_s^i) = \sigma^* \nabla_x (\log \Phi(s, X_s^i))$ when $R \equiv \sigma \sigma^*$. Therefore, in contrast to (5), the unnormalized weights of the nPF are

$$\widehat{w}_{k+1}^i = \frac{d\mu^i}{d\widehat{\mu}^i} \Big|_{t_{k+1}} w_k^i p_k(Y_{k+1} | X_{k+1}^i). \quad (12)$$

For additional details on the nPF, more advanced versions, and its application to higher-dimensional mathematical models than given in this manuscript, we direct the reader to some of the recent literature [25], [26], [27].

1) *Adaptive Nudging Calculation:* Numerical implementation of the nPF requires an approximation of (9) and (10), which is most directly accomplished via MC. To ensure that our approximation of the expectations and hence the control solution has converged to an acceptable tolerance level, an adaptive scheme is used whereby we calculate the control for an increasing number of realizations $(\eta_{k+1}^{k,x})$. This is implemented in batch form to improve efficiency and reuse previously computed realizations. In particular, let $K \in \mathbb{N}$ be a batch size and $j \in \mathbb{N}$ the j -th iteration of the algorithm to compute the control approximation u_t^{jK} , with jK total realizations. Additionally, let

$$\hat{u}_t^{jK} \equiv u_t^{jK} / |\mathbb{E}[f(X_t)]| \quad (13)$$

be the normalized control magnitude. Repeating this approximation for the $(j+1)$ -th iteration, we define the normalized control variation to be

$$\delta \hat{u}_t^{j+1} \equiv |\hat{u}_t^{(j+1)K} - \hat{u}_t^{jK}|. \quad (14)$$

Then for a user specified tolerance $\epsilon_u > 0$, if $\delta \hat{u}^{j+1} \leq \epsilon_u$, the approximate control solution $\hat{u}_t^{(j+1)K}$ is said to have converged, and otherwise we proceed to the $(j+2)$ -th iteration of the algorithm.

2) *Additional Remarks:* We finish this section by making clear the distinction between the nPF and flow-based PF algorithms mentioned in §I, and in particular those derived also from a control perspective such as the feedback particle filter (FPF) [11]. The main distinction is that the FPF applies a control law in the pseudo-observation interval for the Bayes' update, whereas the nPF applies a control to the particles between observations. Since the control in the nPF

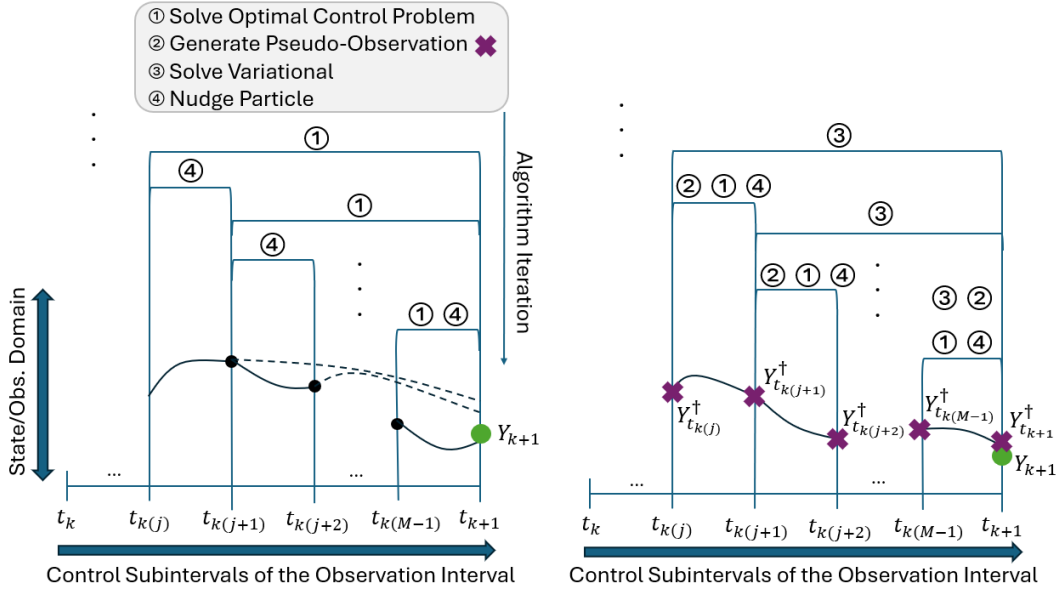


Fig. 2: Schematic evolution of a single particle within one observation interval for the nPF (left) and the Var-nPF (right).

occurs between observations, the weights must be changed accordingly.

Another approach that is closely related to the nPF, but motivated by large deviation theory and derived from a variational method approach, has been applied to a model for the rare event of the Kuroshio current [28].

III. VARIATIONAL NUDGED PARTICLE FILTER

It is not practical to solve for a continuous-time control of the nPF at every time $t \in [t_k, t_{k+1})$ between observations. Therefore, the standard implementation is to partition the interval between observations into $M \in \mathbb{N}$ equal-length control subintervals with a collection of endpoints defining them given by the indexed set $(t_{k(j)})_{j=0}^M$. Then a control solution is found for the time $t_{k(j)}$ at the beginning of each subinterval, by solving the nonlinear OCP in (7) from $t_{k(j)}$ to t_{k+1} , and this control is then held constant in application for the remainder of the subinterval $[t_{k(j)}, t_{k(j+1)})$. As the expectations in (9) and (10) are over the state $\eta_{k+1}^{k,x}$ at the final time, the earlier control subintervals are computationally more expensive (i.e., longer numerical integration times) than the later ones; this is shown in Fig. 2 (left). Additionally, the earlier subintervals are more sensitive to the nonlinear dynamics and noise perturbations, which requires larger batch sizes in the adaptive nudging calculation described in §II-B1.

The central contribution of this paper is to introduce a pseudo-observation path that enables a fixed computational cost for the nudging control in every subinterval. This pseudo-observational path also appears to help moderate the weight variance due to the Radon-Nikodym derivative for the nPF as given in Corollary II.1.

For clarity of discussion, let us fix a single observation interval $[t_k, t_{k+1})$ with observation Y_{k+1} and particles (X_t^i)

(refer to Fig. 2 (right)). We then aim to find the most likely path of the observation; that is a path $(Y_t^\dagger)_{t \in [t_k, t_{k+1}]}$ such that $Y_{t_{k+1}}^\dagger \approx Y_{k+1}$. This likely observation path can then be substituted into (9) and (10) so that control solutions at each subinterval can be calculated with realizations ending at the end of the subinterval, $t_{k(j+1)}$, instead of the full observation interval, t_{k+1} . To find such a likely observation path, we instead solve for a state-space path (X_t^\dagger) that is the most likely path from a given initial condition to a state that generates the observation Y_{k+1} . In particular, this state-space path is found by solving a variational problem. Specifically, what is often referred to as the strong constraint 4-dimensional variational (sc4DVar) approach in the geophysical data assimilation community [3], [7], [8]. The optimization problem to be solved is

$$\min_{x \in \mathbb{R}^m} \left\{ J(x; k, Y_{k+1}) \equiv \frac{1}{2} \langle \Delta x, (\Sigma_k^N)^{-1} \Delta x \rangle + \frac{1}{2} \langle \Delta y, \Sigma_y^{-1} \Delta y \rangle \right\}, \quad (15)$$

with μ_k^N and Σ_k^N an empirical mean and covariance respectively (e.g., for the nPF solution) at time t_k , $\Delta x \equiv x - \mu_k^N$, $\Delta y \equiv Y_{k+1} - h(X_{k+1}^{k,x})$ is the innovation, where $X_{k+1}^{k,x}$ is the solution of the deterministic dynamics (i.e., $\sigma = 0$ in (1)). If (X_t^\dagger) is now the most likely path integrated under the deterministic dynamics, starting from an optimal solution to (15), then the pseudo-observation path is simply $Y_t^\dagger \equiv h(X_t^\dagger)$.

In the case where the measurement operator is simply the identity mapping (i.e., h is the identity matrix $\text{Id.} \in \mathbb{R}^{m \times m}$), then the observation and state-space are identical, and we can use X_t^\dagger as the pseudo-observation path itself. We note that it is natural to also extend (15) to the case of multiple

observation at different times, but in this work we only consider assimilation cycles with one observation time.

A. The Variational Nudged Particle Filter Algorithm

The combination of the variational approach with the nPF now proceeds by first computing a solution to the variational problem of (15) for a given control subinterval described in §III. Advecting the a deterministic state starting from this optimal initial condition to the end of the control subinterval generates a target pseudo-observation $Y_{t_{k(j+1)}}^\dagger$ that is then used as a conditional parameter (pseudo-observation) to the nPF OCP in Theorem II.1. These pseudo-observations are shown in Fig. 2 (right).

As discussed at the beginning of this section, the nudged control problem is now always of fixed time duration, being equal to the subinterval length $t_{k(j)} - t_{k(j+1)}$. We repeat this procedure for each control subinterval, including the final one, where we still use the produced pseudo-observation $Y_{t_{k+1}}^\dagger$ instead of the true given one Y_{k+1} . This new algorithm is labeled Var-nPF throughout the remainder of the paper.

For the numerical experiments given in §IV, the optimization of the variational problem given by (15) is solved with a bounded limited Broyden-Fletcher-Goldfarb-Shannon (L-BFGS-B) [29]. In the case that Σ_k^N is poorly conditioned, we add a small regularization term $\epsilon \text{Id.}$, with $0 < \epsilon \ll 1$.

IV. NUMERICAL EXPERIMENTS

In this section we first explain the setup of a stochastic version of the L63 model [30] to be used in experiments, then pertinent simulation parameters, and lastly the findings and comparisons of individual and MC experiments.

A. The Stochastic Lorenz 1963 Model

The deterministic definition of the L63 model [30] has a drift vector field f for (1) given by

$$f : (x, y, z) \mapsto (\alpha(y - x), \gamma x - y - xz, xy - \beta z), \quad (16)$$

where standard parameters are $\alpha = 10, \gamma = 28, \beta = 8/3$, and are used in this work. With these parameters the L63 model is chaotic and solutions converge onto an attractor as shown in Fig. 1. The error doubling time, an indicator of how chaotic a system is, is approximately 0.76 time units (TU), and the average time that a solution switches from one lobe of the attractor to the other is approximately 1.75 TU.

The nPF requires a stochastic dynamical system for its application. We therefore modify the L63 model by adding the stochastic forcing shown in (1). In particular, we consider the additive noise case, where the dispersion coefficient σ is constant and defined so that the diffusion coefficient for the stochastic forcing is

$$\sigma\sigma^* \equiv \begin{bmatrix} 2 & 1 & 0.5 \\ 1 & 2 & 1 \\ 0.5 & 1 & 2 \end{bmatrix}. \quad (17)$$

B. Simulation Parameters

All simulations will use $N = 10$ particles, observation step-size $\Delta t_{\text{obs}} = 0.5$ TU, and final time $t_f = 3.5$ TU. Numerical intergration is with a Wiener-RK4-Maruyama scheme, with integrator step-size $\Delta t = 0.01$ TU. Unless stated otherwise, the initial condition is chosen as $x = (1.508870, -1.531271, 25.46091)$, which is identified in Fig. 1 by the red star.

The initial particle ensembles for any PF method is via sampling from a Gaussian $\mathcal{N}(\mu, 2\text{Id.})$, where μ represents one of the initial conditions shown in Table III and labeled on the attractor in Fig. 1. These representative initial conditions were generated from a long deterministic trajectory of the attractor with the aim to provide low-discrepancy samples of the attractor itself. These initial conditions therefore provide dynamically distinct states and promote MC results that provide a fairer benchmarking of the various filtering methods.

The observation operator is $h = \text{Id.}$ with noise covariance $\Sigma_y = 2\text{Id.}$, so that the standard deviation of the observation noise is less than 5% of the characteristic range of the L63 state variables. This ensures that the observations are informative without dominating the model dynamics.

Each observation interval is partitioned into $M = 5$ control subintervals. In the solution of the OCP for each subinterval, we use $K = 2$ trajectory realizations per batch together with the adaptive nudging strategy described in §II-B1. A tolerance of $\epsilon_u = 0.1$ is used for the adaptive nudging calculation. A maximum of 50 batches (i.e., 100 total realizations) is allowed in the calculation, though none of the experiments required this many to converge to our tolerance of ϵ_u .

C. Simulation Results

We first consider a fixed simulation scenario to illustrate the prototypical behavior of the PF, nPF, and Var-nPF methods. Then having established and visualized the behavior of these methods, we perform a MC analysis.

Prototypical Behavior: To better understand and visualize particle motion within a single observation interval across the three PF variants presented in this work, we consider the case where all filters use the same samples generated from a Gaussian distribution with mean given by the red star in Fig. 1. These samples are shown by gray circle markers in Fig. 3, where they have been projected onto the dominate subspace spanned by the prior states of all the particles (i.e., all the methods) at the first observation time. This subspace is found by a singular value decomposition of a matrix with all the particle states as columns.

All three methods perform filtering with the same true hidden signal (black line) and observations (green markers) as shown in Fig. 4. Fig. 3 shows the prior particle locations with triangular markers, and the size of the markers is a reflection of each particles normalized weight. In particular, the PF does not change the weights of the particles, whereas the nPF and Var-nPF weights do change as the particles attempt to nudge closer to the observation. The PF normalized ESS (nESS) changes from 1 for the prior to 0.15 after the Bayes' update, where as

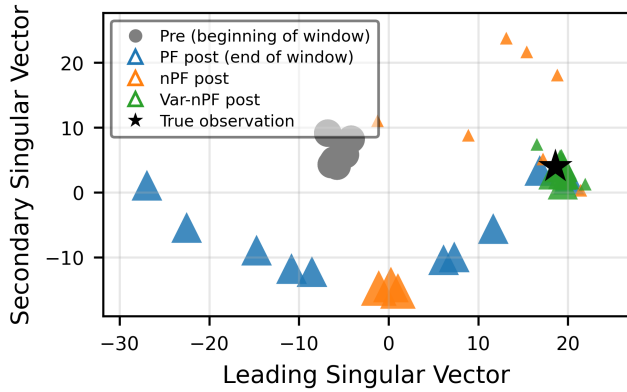


Fig. 3: Initial particle samples for all methods shown with gray circle markers. Prior states of each method (triangles) at the first observation $t = 0.5$ scaled to the normalized weight.

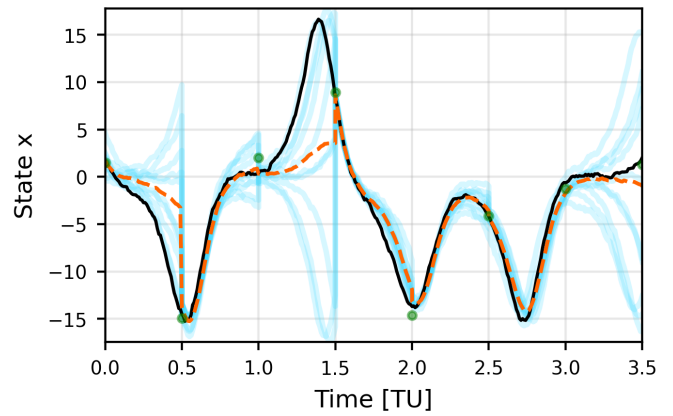
the nPF goes from 0.3 to 0.1, and the Var-nPF from 0.56 to 0.41.

While the PF spreads significantly after advection, the nPF, and especially those of the Var-nPF, move toward the observation. This observation interval corresponds to a “rare” event (i.e., a transition of the lobes), as shown in Fig. 4. It is for this reason that the PF, which has no control, ends up with too much variance at the time of the observation. It is promising that all of the Var-nPF particles arrive in the area of high likelihood for the observation, and most with reasonably good weights. We see this behavior also holds true for other switching times between lobes in Fig. 4.

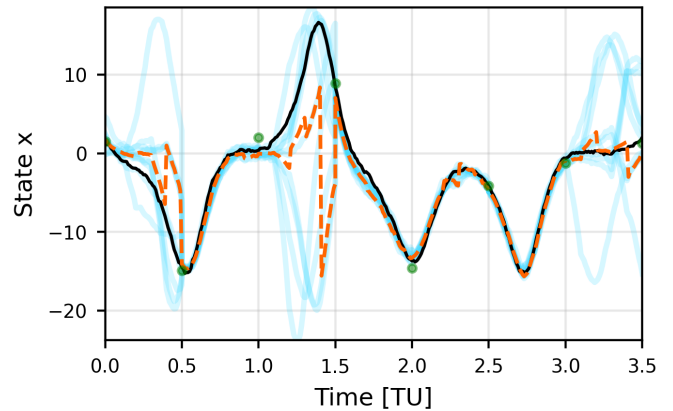
The nPF particles that do not arrive near the observation is due to our implementation that prevents nudging to occur if it would reduce an individual particles unnormalized weight too much. We refer to such cases in this paper as a “zero control rollback” (i.e., we calculate the proposed control, but ultimately do not apply it—see Table I).

It is interesting to compare the nudging control magnitude relative to the BM vector field (VF) as shown in Fig. 5 for this experiment. This relative nudging to BM VF is shown in green for each particle and the ensemble mean in blue. The nESS is shown with the second y-axis in orange.

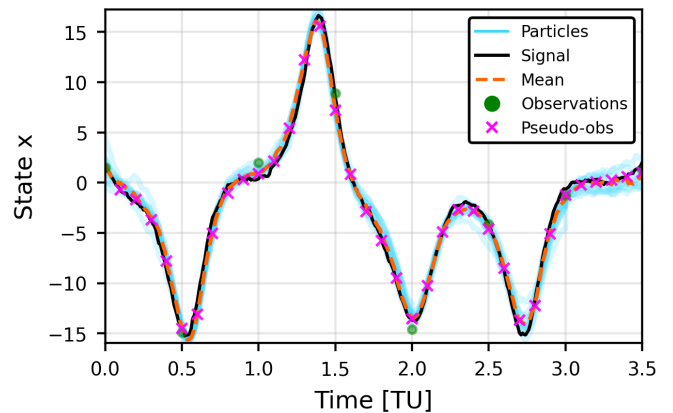
Of particular note is the aggressive control of the nPF, whereas our new method is able to relax the proposed relative control and hence deliver more particles to the observation location and with better nESS. This is most easily observed from the ensemble mean of the nudging relative to the BM VF taking larger values (above the upper bound of the plot) for the nPF, but only at the end of the simulation for the Var-nPF. These occurrences correspond to larger dispersion in the particles at those times, which can be seen in Fig. 4. It is important to note that the nudging to BM VF ratio should remain below a value of one on average if we are to believe that the stochastic model is properly defined (i.e., if the stochastic forcing represents model uncertainty, then it is parameterized properly to reflect reality and our filtering method is not trying



(a) PF



(b) nPF



(c) Var-nPF

Fig. 4: Time evolution of the first state component (i.e., x).

to overpower the model defined dynamics). We indeed see this to happen more often in the new Var-nPF, which is a promising indicator.

The computational overhead introduced by the variational component was also analyzed for this experiment and MC runs, which showed similar trends. In particular, solving the variational problem accounts for approximately 40.5% of the

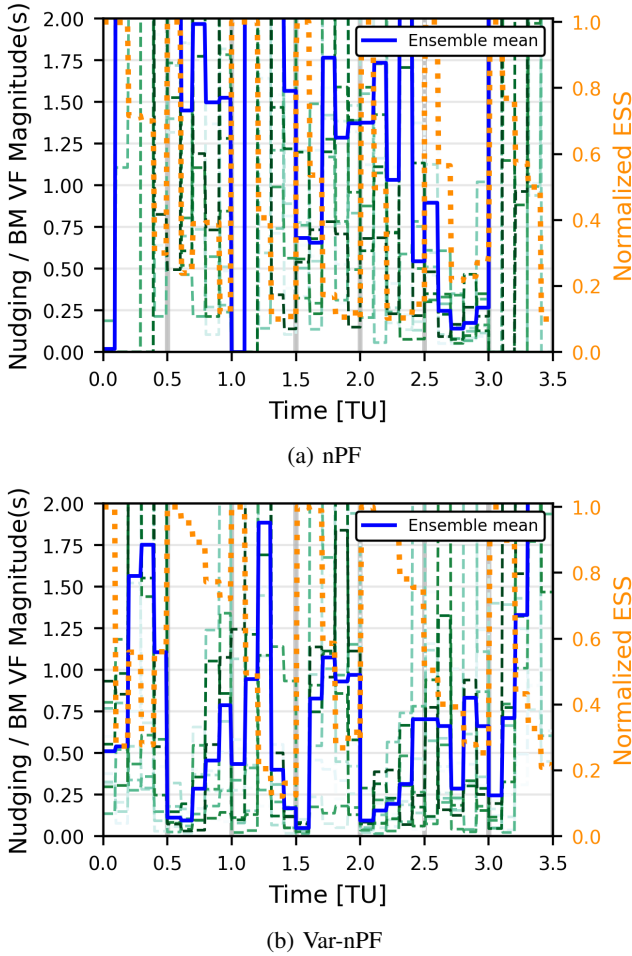


Fig. 5: Nudging magnitude relative to BM forcing (green), ensemble mean for this relative control (blue), and the nESS.

TABLE I: Comparison between PF, nPF, and Var-nPF for one experiment with the red star initial mean condition.

Metric	nPF	Var-nPF
Mean of Control Magnitude $\ u\ _2$	18.14	4.55
Maximum of Control Magnitude $\ u\ _2$	220.91	41.13
Fraction of Zero Control Rollback	0.166	0.000
Average Nudging / BM VF ratio	2.87	0.77
Maximum Nudging / BM VF ratio	60.62	9.69
Average RMSE	4.92	1.48
Runtime (s)	13.49	7.8

total Var-nPF runtime. The remaining run time was due to the nPF control calculations. Although the variational component constitutes a significant portion of the computation, it does not dominate the overall runtime and reduces the computational cost compared to the nPF for this experiment (see Table I). As long as a decent optimization solution is provided by the variational part of the new method, it has the potential to scale much better for higher dimensional and longer observation interval problems. The average Root Mean Square Error (RMSE) for each method shown in Table I, is the average over the state and time with respect to the true signal.

TABLE II: 100 MC runs; red star initial mean in Fig. 1

Metric	Filter Type				
	PF ₁₀	PF ₃₀	PF ₄₀	nPF	Var-nPF
Number of Particles	10	30	40	10	10
Avg. RMSE	6.35	4.47	3.66	6.39	2.91
Normalized Avg. ESS	0.27	0.26	0.27	0.17	0.26
Runtime (s)	18.47	30.45	37.21	283.9	132.92

TABLE III: MC (1000 total runs, 100 for each μ initial condition), reporting Avg. nESS, Avg. RMSE, and runtime.

#	μ Initial Condition	PF		nPF		Var-nPF	
		nESS	RMSE	nESS	RMSE	nESS	RMSE
*	(1.509, -1.531, 25.461)	0.27	6.35	0.17	6.39	0.26	2.91
1	(-3.622, 2.487, 29.784)	0.26	6.64	0.14	8.34	0.25	4.37
2	(-8.587, -14.288, 16.895)	0.30	6.83	0.20	6.43	0.27	4.64
3	(-14.411, -8.058, 40.440)	0.26	6.50	0.17	5.79	0.24	4.45
4	(14.418, 11.236, 37.915)	0.25	7.96	0.18	5.69	0.24	6.17
5	(4.133, 6.815, 14.316)	0.28	8.02	0.19	7.75	0.26	5.35
6	(-2.895, -5.123, 11.843)	0.32	5.57	0.19	5.47	0.27	3.98
7	(-5.802, -7.589, 20.507)	0.36	4.00	0.22	3.70	0.31	2.94
8	(10.347, 17.701, 17.250)	0.25	8.86	0.16	7.42	0.24	5.41
9	(3.072, -0.052, 26.056)	0.25	7.96	0.14	8.80	0.25	4.28
10	(1.909, -0.842, 24.846)	0.22	10.31	0.17	6.76	0.26	2.98
Avg.	—	0.28	7.27	0.18	6.62	0.26	4.46
Avg.	Computational Runtime	23.39		202.08		129.87	

Monte Carlo Simulations: To validate that the trends and observations seen in the single experiment described in the last section hold in general, we performed a MC analysis of 100 simulations with the red star initial condition (see Fig. 1) as the mean of a Gaussian to be sampled. These MC results are given in Table II and it shows that the nPF improves the average RMSE slightly over the PF, but with degradation in the nESS. The limiting factor in the performance of the nPF to achieve better RMSE is due to the fact that we only use $M = 5$ control subintervals, which therefore results in the non-insignificant fraction of zero control rollbacks detailed in Table I. Using more control subintervals would drastically increase the runtime of the nPF, which was already deemed high for comparisons to the PF for this low-dimensional model.

There is noticeable improvement in the the RMSE for the new Var-nPF without a degradation in the nESS. Table I also shows MC results for the PF with an increasing number of particles, so that a better comparison of the performance of the methods on an estimation accuracy and computational runtime level can be made. Although the Var-nPF achieves the best average RMSE it is likely still computationally more expensive for a PF method with a sufficiently high number of particles (e.g., it seems that 50 to 60 particles may suffice to achieve the same RMSE but with half the run time). We hypothesis that the estimation accuracy and computational runtime will be more favorable for the new method in future testing of higher dimensional models.

To further validate that the trends and observations hold generally for the application of the methods to the stochastic L63 model, we perform another MC simulation, but with 100 runs for each of the 10 initial means given in Table III and labeled in Fig. 1. The PF exhibits a consistently low

nESS and relatively large RMSE, indicating significant weight degeneracy. The nPF improves the estimation accuracy in several cases, but does not reduce the estimation error across all initial conditions. Notably, the new Var-nPF approach achieves consistently lower RMSE, demonstrating improved robustness with respect to variations in the initial state of the L63. These results indicate that incorporating the modified variational approach enhances the accuracy of the filtering process. The computational runtime trends from Table II are maintained in this MC experiment, as shown by the last row of Table III.

V. CONCLUSIONS

In this paper, we have introduced a variational pseudo-observation guided nPF for filtering nonlinear chaotic systems with sparse observations that may exhibit “rare” events. By generating intermediate pseudo-observations within each observation interval, the proposed approach replaces long time-horizon OCPs with shorter ones. Numerical results on the stochastic L63 show that the Var-nPF improves estimation accuracy relative to both PF and nPF while reducing computational cost. This provides gentler nudging of the particles in each subinterval, enabling more consistent control and promoting better weight diversity.

The observation interval used in this work was shorter than the average switching time between lobes of the L63 attractor. To better mimic a “rare” event, future work will test on longer duration regimes that are more comparable to the switching timescale. This setting will better test the sensitivity of the variational component of the Var-nPF.

Future efforts will also investigate the use of regularized variational methods [31], as well as test the Var-nPF on higher-dimensional systems such as the Lorenz 1996 model [32] and geophysical models demonstrating observed rare events [6].

REFERENCES

- [1] P. J. van Leeuwen, H. R. Künsch, L. Nerger, R. Potthast, and S. Reich, “Particle filters for high-dimensional geoscience applications: A review,” *Quarterly Journal of the Royal Meteorological Society*, vol. 145, no. 723, pp. 2335–2365, 2019. [Online]. Available: <https://rmets.onlinelibrary.wiley.com/doi/abs/10.1002/qj.3551>
- [2] C. Snyder, T. Bengtsson, P. Bickel, and J. L. Anderson, “Obstacles to high-dimensional particle filtering,” *Monthly Weather Review*, vol. 136, no. 12, pp. 4629–4640, 2008.
- [3] G. Evensen, F. C. Vossepoel, and P. J. van Leeuwen, *Data Assimilation Fundamentals: A Unified Formulation of the State and Parameter Estimation Problem*. Springer International Publishing, 2022. [Online]. Available: <https://doi.org/10.1007/978-3-030-96709-3>
- [4] J. A. Bucklew, *Introduction to Rare Event Simulation*. New York, NY: Springer New York, 2004. [Online]. Available: <https://doi.org/10.1007/978-1-4757-4078-3>
- [5] E. Vanden-Eijnden and J. Weare, “Rare event simulation of small noise diffusions,” *Communications on Pure and Applied Mathematics*, vol. 65, no. 12, pp. 1770–1803, 2012. [Online]. Available: <https://onlinelibrary.wiley.com/doi/abs/10.1002/cpa.21428>
- [6] B. Qiu and W. Miao, “Kuroshio path variations south of japan: Bimodality as a self-sustained internal oscillation,” *Journal of Physical Oceanography*, vol. 30, no. 8, pp. 2124 – 2137, 2000. [Online]. Available: https://journals.ametsoc.org/view/journals/phoc/30/8/1520-0485_2000_030_2124_kpvsoj_2.0.co_2.xml
- [7] O. Talagrand and P. Courtier, “Variational assimilation of meteorological observations with the adjoint vorticity equation. i: Theory,” *Quarterly Journal of the Royal Meteorological Society*, vol. 113, no. 478, pp. 1311–1328, 1987. [Online]. Available: <https://rmets.onlinelibrary.wiley.com/doi/abs/10.1002/qj.49711347812>
- [8] P. Courtier and O. Talagrand, “Variational assimilation of meteorological observations with the adjoint vorticity equation. ii: Numerical results,” *Quarterly Journal of the Royal Meteorological Society*, vol. 113, no. 478, pp. 1329–1347, 1987. [Online]. Available: <https://rmets.onlinelibrary.wiley.com/doi/abs/10.1002/qj.49711347813>
- [9] F. Daum and J. Huang, “Nonlinear filters with log-homotopy,” in *Signal and Data Processing of Small Targets 2007*, O. E. Drummond and R. D. Teichgraber, Eds., vol. 6699, International Society for Optics and Photonics. SPIE, 2007, p. 669918. [Online]. Available: <https://doi.org/10.1117/12.725684>
- [10] U. D. Hanebeck, K. Briechle, and A. Rauh, “Progressive Bayes: a new framework for nonlinear state estimation,” in *Multisensor, Multisource Information Fusion: Architectures, Algorithms, and Applications 2003*, B. V. Dasarathy, Ed., vol. 5099, International Society for Optics and Photonics. SPIE, 2003, pp. 256 – 267. [Online]. Available: <https://doi.org/10.1117/12.487806>
- [11] T. Yang, P. G. Mehta, and S. P. Meyn, “Feedback particle filter,” *IEEE Transactions on Automatic Control*, vol. 58, no. 10, pp. 2465–2480, 2013.
- [12] A. Spantini, R. Baptista, and Y. Marzouk, “Coupling techniques for nonlinear ensemble filtering,” *SIAM Review*, vol. 64, no. 4, pp. 921–953, 2022. [Online]. Available: <https://doi.org/10.1137/20M1312204>
- [13] S. Reich, “Data assimilation: The schrödinger perspective,” *Acta Numerica*, vol. 28, pp. 635–711, 2019.
- [14] A. J. Chorin and X. Tu, “Implicit sampling for particle filters,” *Proceedings of the National Academy of Sciences*, vol. 106, no. 41, pp. 17249–17254, 2009. [Online]. Available: <https://www.pnas.org/doi/abs/10.1073/pnas.0909196106>
- [15] G. Evensen, “Sequential data assimilation with a nonlinear quasi-geostrophic model using monte carlo methods to forecast error statistics,” *Journal of Geophysical Research: Oceans*, vol. 99, no. C5, pp. 10143–10162, 1994. [Online]. Available: <https://agupubs.onlinelibrary.wiley.com/doi/abs/10.1029/94JC00572>
- [16] G. Burgers, P. J. van Leeuwen, and G. Evensen, “Analysis scheme in the ensemble kalman filter,” *Monthly Weather Review*, vol. 126, no. 6, pp. 1719 – 1724, 1998. [Online]. Available: https://journals.ametsoc.org/view/journals/mwre/126/6/1520-0493_1998_126_1719_asitek_2.0.co_2.xml
- [17] S. Julier and J. Uhlmann, “Unscented filtering and nonlinear estimation,” *Proceedings of the IEEE*, vol. 92, no. 3, pp. 401–422, 2004.
- [18] H. Sorenson and D. Alspach, “Recursive bayesian estimation using gaussian sums,” *Automatica*, vol. 7, no. 4, pp. 465–479, 1971. [Online]. Available: <https://www.sciencedirect.com/science/article/pii/0005109871900975>
- [19] N. Lingala, N. Perkowski, H. C. Yeong, N. S. Namachchivaya, and Z. Rapti, “Optimal nudging in particle filters,” *Probabilistic Engineering Mechanics*, vol. 37, pp. 160–169, July 2014. [Online]. Available: <https://doi.org/10.1016/j.probenmech.2013.08.007>
- [20] H. C. Yeong, R. T. Beeson, N. S. Namachchivaya, and N. Perkowski, “Particle filters with nudging in multiscale chaotic systems: With application to the lorenz ’96 atmospheric model,” *Journal of Nonlinear Science*, vol. 30, no. 4, pp. 1519–1552, 2020.
- [21] N. J. Gordon, D. J. Salmond, and A. F. M. Smith, “Novel approach to nonlinear/non-Gaussian Bayesian state estimation,” *IEE Proceedings F - Radar and Signal Processing*, vol. 140, no. 2, pp. 107–113, 1993.
- [22] N. Bergman, “Recursive bayesian estimation: Navigation and tracking applications,” Ph.D. dissertation, Linköping University, Linköping, Sweden, 1999. [Online]. Available: <https://www.rt.isy.liu.se/research/reports/Ph.D.Thesis/PhD579.pdf>
- [23] J. S. Liu and R. Chen, “Sequential monte carlo methods for dynamical systems,” *Journal of the American Statistical Association*, vol. 93, no. 433, pp. 1032–1044, 1998. [Online]. Available: <http://www.jstor.org/stable/2669847>
- [24] G. Kitagawa, “Monte carlo filter and smoother for non-gaussian nonlinear state space models,” *Journal of Computational and Graphical Statistics*, vol. 5, no. 1, pp. 1–25, 1996. [Online]. Available: <http://www.jstor.org/stable/1390750>

- [25] R. Beeson and N. Sri Namachchivaya, "Particle filtering for chaotic dynamical systems using future right-singular vectors," *Nonlinear Dynamics*, vol. 102, pp. 679–696, 2020.
- [26] R. Beeson and U. Hanebeck, "Nudged particle filter with optimal resampling applied to the duffing oscillator," in *28th International Conference on Information Fusion (FUSION)*, 7 2025, pp. 1–8.
- [27] B. Zhou and R. Beeson, "Projected feedback particle filtering for chaotic dynamical systems using lyapunov vectors," in *2024 27th International Conference on Information Fusion (FUSION)*, 2024, pp. 1–8. [Online]. Available: <https://doi.org/10.23919/FUSION59988.2024.10706376>
- [28] E. Vanden-Eijnden and J. Weare, "Data assimilation in the low noise regime with application to the kuroshio," *Monthly Weather Review*, vol. 141, no. 6, pp. 1822 – 1841, 2013. [Online]. Available: <https://journals.ametsoc.org/view/journals/mwre/141/6/mwr-d-12-00060.1.xml>
- [29] "Scipy optimization." [Online]. Available: <https://docs.scipy.org/doc/scipy/tutorial/optimize.html>
- [30] E. N. Lorenz, "Deterministic nonperiodic flow," *Journal of the Atmospheric Sciences*, vol. 20, no. 2, pp. 130–141, 1963.
- [31] Y. Trémolet, "Accounting for an imperfect model in 4d-var," *Quarterly Journal of the Royal Meteorological Society*, vol. 132, no. 621, pp. 2483–2504, 2006.
- [32] E. N. Lorenz, "Predictability: A problem partly solved," *Proc. Seminar on Predictability*, 1996.